Soft Matter

Accepted Manuscript

This article can be cited before page numbers have been issued, to do this please use: E. Sabattié, J. Tasche, M. R. Wilson, M. W. A. Skoda, A. V. Hughes, T. Lindner and R. Thompson, *Soft Matter*, 2017, DOI: 10.1039/C7SM00048K.

ROYAL SOCIETY OF CHEMISTRY

rsc.li/soft-matter-journal

View Article Online
DOI: 10.1039/C7SM00048K

Journal Name

ARTICLE

Received 00th January 20xx,
Accepted 00th January 20xx

DOI: 10.1039/x0xx00000x

www.rsc.org/

Predicting Oligomer/Polymer Compatibility the Impact on Nanoscale Segregation in Thin Films.

Elise F. D. Sabattié[a,b], Jos Tasche[a], Mark R. Wilson[a], Maximilian W. A. Skoda[c], Arwel Hughes[c], Torsten Lindner[b] and Richard L. Thompson[a,*]

Compatibility between oligomers and polymers was systematically assessed using differential scanning calorimetry (DSC) and was correlated with similarity in saturation and solubility parameter. These measurements enabled validation of detailed volume of mixing calculations using Statistical Association Fluid Theory (SAFT-γ Mie) and molecular dynamics (MD) simulations, which can be used to predict behaviour beyond the experimentally accessibly conditions. These simulations confirmed that squalane is somewhat more compatible with poly(isoprene), "PI" than poly(butadiene), "PB", and further enabled prediction of the temperature dependence of compatibility. Surface and interfacial segregation of a series of deuterated oligomers was quantified in rubbery polymer films PI, PB and hydrogenated poly(isoprene) "hPI". A striking correlation was established between surface wetting transition and mixtures of low compatibility, such as oligo-dIB in PB or PI. Segregation was quantified normal to the surface by ion beam analysis and neutron reflectometry and in some cases lateral segregation was observable by AFM. While surface segregation is driven by disparity in molecular weight in highly compatible systems this trend reverses as critical point is approached, and surface segregation increases with increasing oligomer molecular weight.

[a] Department of Chemistry, Durham University, Science Site, Durham DH1 3LE, U.K.
[b] Procter & Gamble, German Innovation Center (GIC), Sulzbacher Str. 40-50, 65824 Schwalbach am Taunus, Germany..
[c] STFC ISIS Facility, Rutherford Appleton Laboratories, Chilton, Didcot, OX110QX, U.K.

Supplementary Information (ESI) available: Fitted parameters to neutron reflectometry experiments, pre-normalisation concentration profiles for d-styrene in hPI and oligo-dIB in PB, and neutron reflectometry analysis of dsq in PI and PB films. See DOI: 10.1039/x0xx00000x

Introduction

Molecular migration, segregation and self-organisation in polymers are ubiquitous processes that govern the processing, performance, and life-time of many industrially important products. These include paints, coatings, packaging and adhesive formulations, and efficient use of materials in these formulations is dependent on understanding of how and when small molecules migrate through a polymer matrix. Here we consider a simple model system that lacks the complexity of polar interactions or hydrogen bonding, yet has sufficiently strong interactions between small molecules and polymer matrices to traverse a phase boundary. This system is directly relevant to hot-melt adhesives (HMAs), which are used in pressure sensitive adhesives applications such as disposable products, stamps and envelopes.[1]

Oligomeric tackifiers are commonly added into HMAs in order to control the glass transition temperature and improve "tack" properties – i.e. ability to adhere to a surface under very slight pressure and. Generally, they are organic oligomers having a molecular weight of order 300-2000 g/mol.[2,3,4] Tackifiers therefore have a relatively high diffusive mobility and may spontaneously segregate (or "bloom") to surfaces or interfaces. Excessive blooming is unwanted in HMA formulations as it can lead to contamination of other materials or decrease the HMA's performance. Interestingly, however, a thin surface layer that is enriched in additive, which might be expected in a single phase system, might be beneficial in improving adhesion.

Additive surface segregation is due to a combination of entropic and enthalpic factors. It has been well established by theory,[5, 6] simulation[7, 8] and experiment[9, 10] that chain ends will be preferentially enriched at a surface. The entropic penalty associated with placing a large polymer chain at a surface is greater than that for a smaller chain. This effect also applies to chain ends when compared to mid-chain segments, and has a significant impact on the adsorption efficiency of low surface energy functional groups[11-13] and bottle-brush structured polymers.[14] Interpretation of the interplay between surface energy and entropic contributions to surface activity has been achieved successfully by Archer et al, using a linear response theory to predict the crossover point at which low molecular weight or branching can overcome a small difference in surface energy, thus promoting surface segregation, even when surface energy arguments alone would preclude this.[15] However, in this work, the accuracy of prediction decreases with decreasing molecular weight and to our knowledge, no such treatment exists yet for the extreme case of segregation

View Article Online
DOI: 10.1039/C7SM00048K

by an oligomer that is too small to be treated as a Gaussian polymer chain.

The extent of surface segregation in polymer blends significantly increases with increasing incompatibility.[16,17] Incompatibility, is most commonly described using Flory-Huggins theory, whereby the free energy density of mixing, ΔG_{mix}, is given by

$$\frac{\Delta G_{mix}}{v_e k_B T} = \frac{\varphi ln\varphi}{N_1 v_1} + \frac{(1-\varphi)ln(1-\varphi)}{N_2 v_2} + \frac{\chi\varphi(1-\varphi)}{v_e} \qquad (1)$$

where N_i and v_i are the number and volume of repeat units in each component, v_e is an (arbitrary) reference volume and ϕ is the volume fraction of component 1. Interactions between unlike components are described by the Flory-Huggins interaction parameter χ.[18,19] Although Flory Huggins theory model has little predictive capacity, and has been superseded by more accurate approaches that use PVT data for the pure components, it provides a convenient framework with which to understand some of the contributions to miscibility.[20]

A fairly compatible system – χ negative or too small to overcome the first two (entropic) terms in equation 1 – exists as a single bulk phase but a surface excess can be observed on a length scale τ, of order of the molecular dimensions given by equation 2 (R_g, Fig. 1 blue curves).

$$\frac{1}{\tau^2} = \frac{\varphi_2}{R_1^2} + \frac{\varphi_1}{R_2^2} \qquad (2)$$

where φ_i is the bulk volume fraction of the *i*-th component and R_i is the characteristic dimension of this component.[21] If χ is sufficiently positive for the third term of equation 1 to dominate, bulk phase separation is expected, along with the formation of a macroscopically thick pure "wetting layer" spreading at the surface of the polymer (Figure 1 pink curve). This distinction between surface segregation and complete wetting can most easily be identified from the surface excess concentration, z^*, defined as

$$z^* = \int_0^\infty \varphi(z) - \varphi_b dz \qquad (3)$$

where φ_b is the bulk concentration adjacent to the surface excess region and $\varphi(z)$ is the depth (z) dependent volume fraction profile of the near surface region. The surface excess provides a measure of the number of molecules per unit area, when divided by the molecular volume of the adsorbing species. The value of z^* also defined the equivalent thickness of a pure adsorbing layer. As the bulk coexistence is approached from the single phase region, the surface excess increases logarithmically.[22] The point at which z^* exceeds the molecular dimensions implies multilayer adsorption, which can be taken to indicate the formation of a wetting layer.

In this report we address the nanometer-scale surface segregation of well-defined oligomers with rubbery polymers in a series of mixtures that are chosen to be relevant to HMAs. The aim of this work is to establish system that is sufficiently simple to test molecular and coarse-grained modelling techniques, yet demonstrates the range of migration and segregation behaviour that is known for complex formulations such as HMAs. The ultimate aim is then identify the key molecular parameters that govern the extent of surface segregation in order to achieve better control and predictive capacity for the surface and interfacial properties and aging behaviour. At present this understanding is lacking and formulations are significantly over-engineered in order to counter the adverse effects of ageing which may arise from molecular migration.

The compatibility of constituents has been systematically analysed, to provide a test data set for computational simulations by γ-SAFT and MD. We have quantified oligomer surface and interfacial segregation for the same mixtures in thin films by elastic recoil detection analysis (ERDA) and neutron reflectometry (NR), and used atomic force microscopy (AFM) to characterize lateral phase separation and to identify the relationship between topography and mechanical properties. Results show that even in these extremely simple models for complex industrial formulations, a surprisingly rich variety of behaviours can result from their interactions.

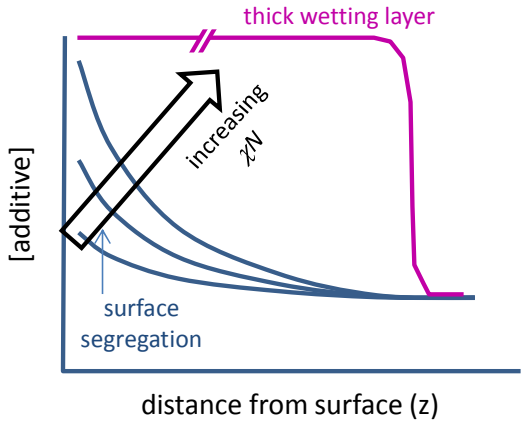

Fig 1 Schematic diagram of the expected evolution of a concentration profile of an additive in a polymer blend near a surface as the incompatibility is increased.

Experimental section

Materials and sample preparation

Polybutadiene (PB) (Sigma-Aldrich P181382, cis-1,4 36%, trans-1,4, 56%, vinyl 8%), polyisoprene (PI) and hydrogenated polyisoprene (hPI) were selected as polymer matrices for the model systems. PI (cis-1,4 80%, trans-1,4, 15%, vinyl 5%[23]), and hPI were synthesized and provided by P&G Cincinnati. Three deuterium labelled model additives were chosen to isolate the effects of saturation and molecular weight on their behaviour. Deuterated squalane "d-sq" was supplied by *Qmx Laboratories*, U.K., D-0958/0.5, $C_{30}D_{62}$ 99% deuterated). Oligo-isobutylene "oligo-dIB" (P18618-d8PIb) and oligo-styrene (oligo-dSTetramer-d33), were all supplied by Polymer Source,

View Article Online
DOI: 10.1039/C7SM00048K

Canada. The deuterium labelling enabled their composition versus depth profiles to be resolved from the polymer matrices by ion beam analysis or neutron reflectometry. The key characteristics of the polymers and oligomers relevant to this study are summarized in Table 1.

Mixed samples of oligomer and polymer, either solid (~ 1 mg) lumps for DSC analysis, or thin (~ 100 nm) films for ion beam analysis and neutron reflectometry were prepared as follows: oligomers and host polymers were dissolved in toluene to create 2 % (w/w) stock solutions. The polymer solutions were left for 1 to 2 days to allow complete dissolution. They were combined in different proportions to obtain 2 wt% solutions in toluene containing the required oligomer : polymer ratio.

Table 1 Physical properties for key components of the model HMA films.

component	M_w /g mol^{-1}	M_w/M_n	n_i	s.l.d. × 10^6 / Å^{-2}
PB $[C_4H_6]_{N_1}$	280 000	2.1	1.5154[24], 1.527[25]	0.416
PI $[C_5H_8]_{N_1}$	160 000	1.1	1.521[24]	0.264
hPI $[C_5H_{10}]_{N_1}$	165 000	1.1	1.475-1.480[25]	-0.32
dsq $C_{30}D_{62}$	423	-	1.4474[26]	6.06
oligo-dS $CD_3[C_8D_8]_{N_2}$	456	-	1.590-1.592[24]	5.72
oligo-dIB $C_8H_{17}[C_4D_8]_{N_2}$	1300	-	1.4813[25]	6.57

Differential scanning calorimetry

Samples for differential scanning calorimetry (DSC) were weighed into standard aluminium pans as mixed solutions, then dried at room temperature overnight. The consistency of T_g values obtained for pure components with established literature values indicated that the solvent (toluene) was successfully removed by this procedure. Analysis was performed using a Perkin Elmer DSC 8000 at a heating rate of 100 °C/min between -130 °C and 120 °C. The heating and cooling cycle was repeated three times to ensure consistency of results.

Thin Film Preparation

Films of 50-200 nm thickness were prepared by spin-coating the mixed solutions onto fresh silicon wafers. Prior to coating, the silicon wafers were cleaned with acetone to remove any traces of hydrophobic impurities and ensure consistent film production.

Elastic recoil detection analysis (ERDA)

ERDA is widely used in to quantify the depth distribution of isotopically labelled polymers in thin films. This technique and its application to similar types of sample is discussed in detail elsewhere.[27, 28] Briefly, a 1.7 MeV 5SDH Pelletron accelerator, (National Electrostatics Corp. Wisconsin USA) was to deliver a 1.5 MeV $^4He^+$ ion beam to each sample. The measurement geometry and settings were similar to our earlier work on related samples.[29] Due to the fact that the films contain molecules of low molecular weight, it was necessary to vitrify the thin film samples before and during ion beam analysis experiments to avoid evaporation. This was achieved by plunging the mounted sample into liquid nitrogen before rapidly transferring the sample to the vacuum system. The sample mount within the RC43 endstation was also cooled to approximately -80 °C via a copper braid connected to a liquid nitrogen filled reservoir. This process also minimises any artefacts arising from radiation-induced cross-linking or chain scission.

IBA data were analysed with the Surrey University DataFurnace[30-32] software (WiNDF v9.3.68 running NDF v9.6a) to determine the concentration versus depth profile, where the densities of PI, PB and hPI were assumed to be ~0.89 g cm^3 and those of squalane, oligo d-S and oligo d-IB 0.81 g cm^3, ~0.9 g cm^3 and ~1 g cm^3 respectively. In order to avoid over-parameterisation, model composition profiles were restricted to a few layers, for which the composition and thickness was allowed to vary to obtain the best possible fit to the experimental data. The fitting procedures used for DataFurnace are described in detail elsewhere.[32-34]

Neutron reflectometry

Sample preparation for neutron reflectivity (NR) was similar to ERDA experiments, except that films were prepared on 55 mm diameter, 5 mm thick silicon blocks instead of thin wafers. The superior depth resolution of NR (0.5 nm) compared to ERDA (~15 nm) enables a more direct test of theoretical predictions of the composition profile. Specular reflectivity, $R(Q)$, was measured using the INTER and SURF reflectometers at ISIS pulsed neutron and Muon source, UK, from before the critical edge (Q ~ 0.01 Å^{-1} for silicon/air) to the point at which the signal is indistinguishable from the background (Q ~ 0.25 Å^{-1}). Here, Q, the scattering vector is defined in the usual way as $Q = (4\pi/\lambda)\sin\theta$, where λ is the neutron wavelength and θ is the scattering angle. The instruments generated largely equivalent data over this range for these samples. Data acquisition on INTER was somewhat more rapid than the other reflectometers due to the large flux and simultaneous Q range. Measurement required at least two angles of incidence and typically 1-2 hours of acquisition time per sample. This latter factor imposes a requirement that films must be stable for several hours, as any alteration in film thickness during measurement would make accurate interpretation of the data impossible.

The scattering length densities (s.l.d's) of the organic components in the film are shown in Table 1, along with literature values for refractive index of the materials or in the case of deterated components, their hydrogenous analogues. The s.l.d. value for the silicon (2.07 x10^{-6} Å^{-2} and the native oxide layer 3.45±0.2 x10^{-6} Å^{-2}) was consistent with results that have been inferred from previous experiments on silicon substrates.[12, 35-37] Fitting of the NR data was performed with the analysis software IGOR Pro, using the Motofit package.[38]

View Article Online
DOI: 10.1039/C7SM00048K

Scanning Probe Microscopy

Lateral variations in the surface properties of thin film samples were studied by scanning probe microscopy using a Bruker MM8 Mulitimode AFM. Samples were prepared in the same way as for ERDA experiments except that smaller (<15 mm) silicon wafer pieces were used. Scans were made with at least 256 line resolution in Peakforce QNM mode at 2 kHz in the vertical direction, and Nanoworld Arrow™ NCR probes with a nominal force constant of 42 Nm^{-1}. Images were analysed using Bruker NanoScope Analysis v1.1 software.

Molecular Dynamics Calculations

Molecular dynamics simulations were carried out in order to determine the change in volume of mixing for mixtures of squalane (sq) with PB and PI. All calculations are performed with the GROMACS 4.6.7 package.[39] The results are obtained from a PB, PI, sq, sq/PB and a sq/PI system at 50% weight fraction for the mixtures. Chain lengths of PB and PI are 12-mers, 819 g/mol and 651 g/mol, respectively. Interactions are described by the TraPPE-UA force field[39-41]. Initial coordinates and GROMACS input files were generated with *Assemble!*[6] A smaller system of 6-7.5k united atom units was equilibrated at 500 K, cooled down to 298 K over 5 ns and further equilibrated for 9 ns, stacked to a cube eight times larger (48-60k united atoms) and further equilibrated for 1 ns. The densities were calculated from averaging over at least 4 ns of simulation time of the stacked up systems at 298 K and 1 bar. All simulations were run in the NPT ensemble, with the Nosé-Hoover thermostat and Parrinello-Rahman barostat applied in the production run. The density of squalane at 298 K agrees with the experimental density[42] to within 0.3%. The magnitude of the relative volumes of mixing are similar to the experimental values of a PB/PI polymer blend.[43]

SAFT-γ Mie

Volumes of mixing and compatibility were modelled with SAFT-γ Mie.[41] Squalane, PI and PB were described with a single interaction type each. The pure component interaction parameters were optimized to reproduce pure component densities over a large range of temperature and pressures[44-46], where the average absolute deviation was minimized. The numbers of beads per chain were chosen to correspond to 2 beads per monomer (considering squalane as a 6-mer) for the number-average molecular weights. Due to the absence of any experimental data, the unlike interactions were not fitted to additional blend data, but purely predicted by combining rules given in Lafitte et al.[42]

Results

Compatibility study

The glass transition (T_g) temperature(s) of oligomer/polymer mixtures was compared to that of the pure components in order to assess the compatibility of the oligomers with the host polymers. The T_gs of a polymer and oligomer in an incompatible system should not change upon mixing since the polymer remains segregated and its local environment is independent of bulk composition. In contrast, a single T_g at an intermediate temperature is usually seen for a compatible mixture. Although there are examples of single phase systems where a double-T_g is observed due to the local environment being perturbed by chain connectivity, these features would still be expected to exist at intermediate temperatures between the T_gs of the pure states.[47] The measured compositional dependence of T_g is shown in Figure 2 as

$$\frac{\mathrm{T_{g,x}} - \mathrm{T_{g,0}}}{\mathrm{T_{g,100}} - \mathrm{T_{g,0}}} = \Delta \mathrm{T_g} \,/\, \Delta \mathrm{T_{g,max}} \qquad (4)$$

where $T_{g,x}$ is the T_g of a oligomer/polymer mixture containing x wt% of oligomer. This representation enables direct comparison of different mixtures by normalising with respect to the T_g's of their pure components. For a miscible blend, the Fox equation (5) predicts the compositional dependence of each mixture's T_g where w_1 and w_2 are the weight fractions of the component 1 and 2, respectively.

$$\frac{1}{T_g} = \frac{w_1}{T_{g,1}} + \frac{w_2}{T_{g,2}} \qquad (5)$$

Figure 2(a) reveals very different trends, corresponding to different levels of compatibility for each model oligomer in hPI. There is almost no effect on the T_g of hPI from blending with 2-80 wt% oligo-dS, which indicates their incompatibility. In contrast, the T_g of hPI mixtures with either dsq or oligo-dIB varies steadily between the extreme values as a function of overall composition. In the case of squalane, the T_g variation is even bigger than that predicted by the Fox equation.

In PI (Figure 2(b)), a substantial T_g variation is recorded when blended with up to 80% dsq, again suggesting a fully miscible system. The effect of blending with oligo-dIB and oligo-dS shows partial compatibility of those oligomers with PI. Finally, in PB, (Figure 2(c)), there is almost no change to the matrix T_g upon loading of oligo-dIB at any of the measured concentrations. The effects of blending dsq with PB are consistent with the Fox equation's predictions for compatible systems. An increase in T_g when the matrix is blended with oligo-dS suggests an intermediate level of compatibility for this pair.

Surface and Interfacial Segregation in Oligomer/Polymer Mixtures

Figure 3 shows that the vertical composition profile of dsq is strikingly sensitive to the polymer matrix in which it is dispersed. Each ERDA spectrum (Fig. 3, inset) shows two clearly resolved peaks, which correspond to the deuterium from the d-labelled oligomer and the protons from the hydrogenous polymer at high and low energy respectively.

View Article Online
DOI: 10.1039/C7SM00048K

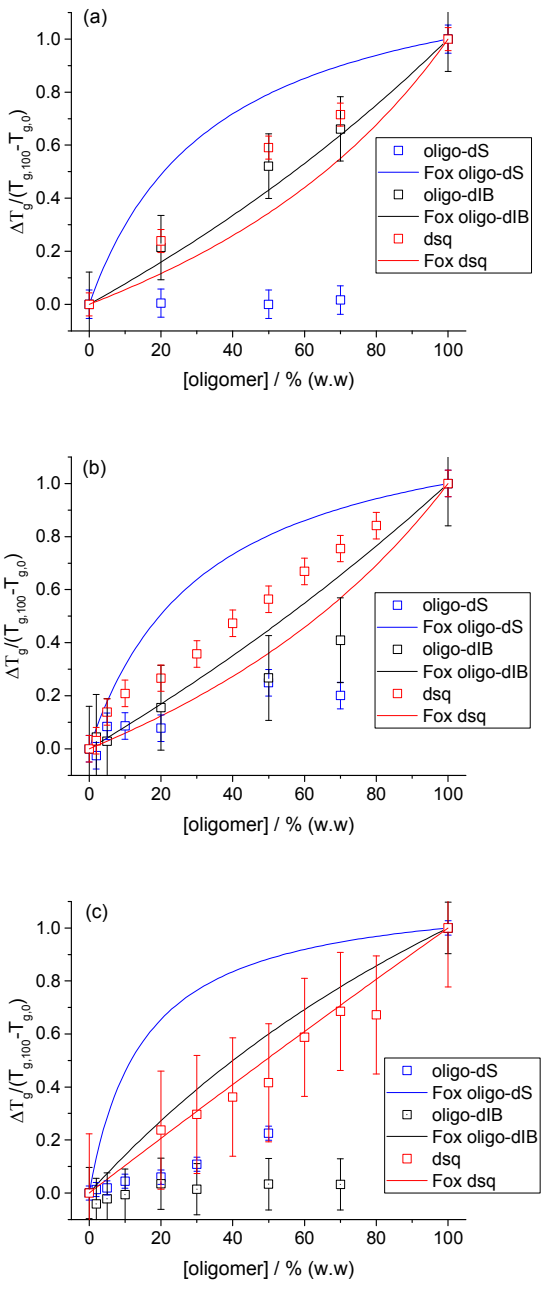

Fig 2 T_g dependence of (a) hPI, (b) PI and (c) PB T_g on composition for mixtures with oligo-dS (blue), 900 g/mol oligo-dIB (black) and dsq (red). Solid lines show the predictions from the Fox equation for each mixture.

Even prior to fitting, it is possible to infer from the data by inspection that dsq shows very different behaviour in the two rubbery polymer matrices. When the H and D peaks are similarly shaped, as is the case for dsq in PI (black), this shows that both the oligomer and the polymer share similar depth distributions, whereas the very different shapes to the peaks for dsq in PB (red) clearly indicates that the oligomer and matrix have different distributions; therefore there is some vertical segregation of these components. The fits to the data in the inset of Figure 3 correspond to the composition profiles shown in the main figure. The ERDA results have high inherent accuracy because they are constrained by known factors such as scattering cross section and stopping power. However, the finite resolution of ERDA means that while the surface excess is well defined (24 ± 3 nm) by the area of the peak in the raw data, the absolute surface concentration is imprecisely measured because the technique cannot distinguish between a very thin, pure surface layer and a thicker, less pure one. For this reason, we have restricted the ERDA analysis to simple layer models. In the thin PI film, the dsq is evenly distributed, whereas it is strongly segregated to the PB film surface.

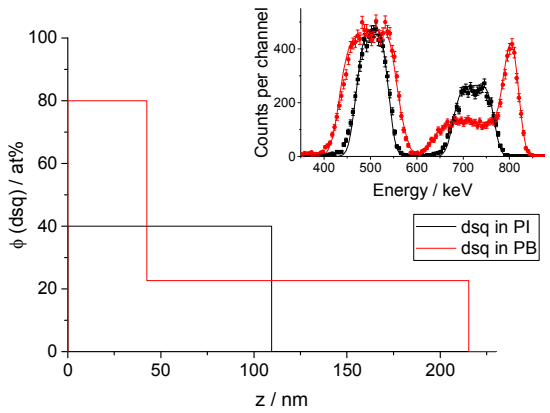

Fig 3 ERDA spectra for 40 wt% dsq in thin PI (black) and PB (red) films. The fitted curves to the data correspond to the composition vs depth profiles of the dsq presented in the inset.

In mixtures of oligo-dS with hPI, the oligomer is found to segregate at the buried interface between the film and the substrate. The ERDA spectra shown in the inset of Figure 4(a) shows that over a broad range of concentrations, an excess of the D signal at the lower energy range, which corresponds to an excess of oligo d-S at the substrate interface, Figure 4(b). The concentration at the surface remains close to zero, and is nearly independent of the overall oligomer concentration. NR measurements on the same materials lead to similar conclusions (Figure 5). The oligomer is segregated at the buried interface while the polymer segregates itself at the surface. Interestingly the shape of the interface does not change much with composition, which is consistent with a low degree of miscibility across a broad range of composition. The depth at which the interface is found is then governed by the overall composition and total film thickness. The profiles obtained by NR confirm that these films have very low surface roughness, ~1 nm, as evidenced by the sharply resolved interference fringes. The fitted parameters are provided as supporting information, S.I.1. Those results are in agreement with Figure 3 (a), showing very little variation of the mixture's T_g, indicating an incompatible system.

View Article Online
DOI: 10.1039/C7SM00048K

ERDA data, fits and derived concentration profiles for the depth distribution of oligo-dIB in PI are presented in Figure 6. Although not as immediately evident as for the dsq / PB films, there is a significant skewing in the proton and deuterium peaks of the spectra. The deuterium recoils due to oligo-dIB are skewed to high energy, implying surface enrichment and the opposite is true for the proton recoils due to the PI. The fits to the experimental data unambiguously show that the oligo-dIB is partially segregated to film surface but that it is unlikely that the surface layer is pure oligo-dIB.

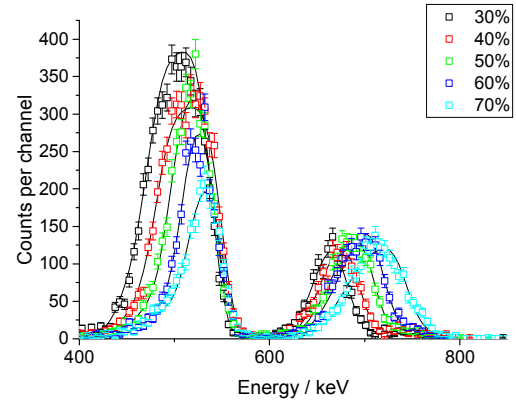

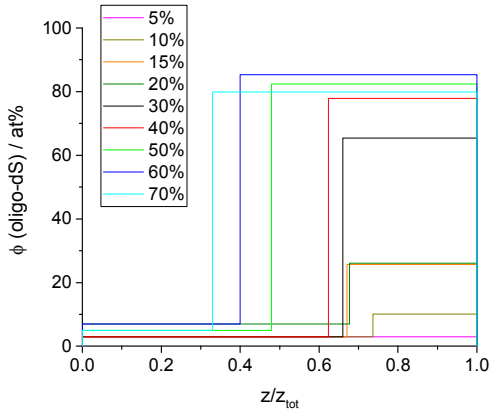

Fig 4 (a) ERDA data and fits for oligo-dS in hPI from 5-70% oligomer concentration. (b) Concentration profiles for d-sty in hPI derived from fits to ERDA data. The depth scale has been normalized for clarity. Profiles with absolute depth scale are included as supporting information S.I.2.

In the oligo-dIB/PI mixtures, where there is significant incompatibility suggested by DSC but only partial vertical inhomogeneity shown by ERDA it is likely that there may be some lateral inhomogeneity in these films too, hence NR was not attempted for these samples. Instead, scanning probe microscopy was applied to films of these components (figure 7) and clearly showed that the surface was not homogeneous,

Fig 5 Concentration profiles for oligo-dS in hPI from 30-50% oligomer concentration derived from fits to NR data (NR data are shown in inset, with fits as solid lines).

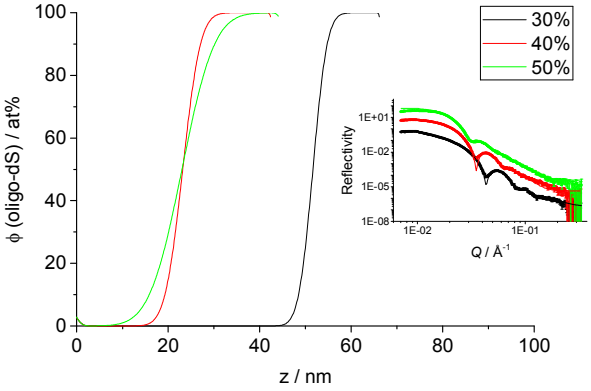

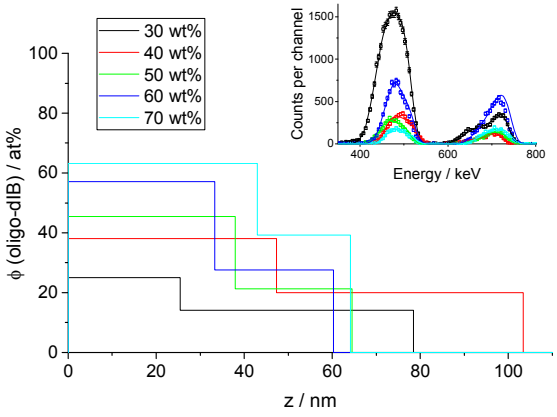

Fig 6 Elastic recoil detection analysis for 30-70 wt% oligo-dIB in thin PI films. The fitted curves to the data (inset) correspond to the composition versus depth profiles of the oligo-dIB presented in the inset.

but instead patchy, with regions of several microns, which are identifiably different in both surface height and adhesion. Although this measurement does not provide a direct mapping of the composition it is usefully able to distinguish between regions that are rich in PI, an elastic solid and oligo-dIB a much softer, tackier material. Since this system is clearly in a two phase regime, the surface excess values become more sensitive to total film thickness than to molecular interactions, so are not analysed here.

A further qualitative change in the behaviour was found for the relatively incompatible combination of oligo-dIB in PB. Figure 2(c) showed that for this combination, the T_g of PB was almost unaffected by the presence of oligo-dIB up to concentrations of 70% oligomer, indicating their strong incompatibility. Thin films of this oligomer/polymer combination were found to exhibit an excess of the oligomer both at the exposed air surface and the buried interface with the silicon substrate. This behaviour is unmistakably apparent from the 'double peak' in the deuterium part of the ERDA spectra (600-800 keV in this case) shown in Figure 8, and is confirmed by the depth profiles obtained from fits to these data.

View Article Online
DOI: 10.1039/C7SM00048K

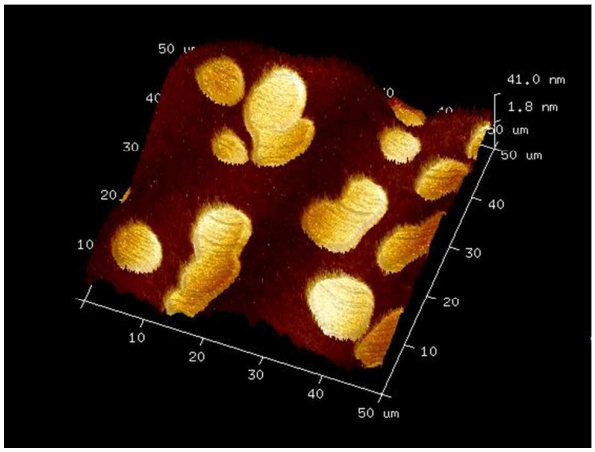

Fig 7 AFM micrograph of thin film comprising 30% oligo-dIB in PI. A false-color 'skin' has been superimposed to highlight regions of relatively high adhesion.

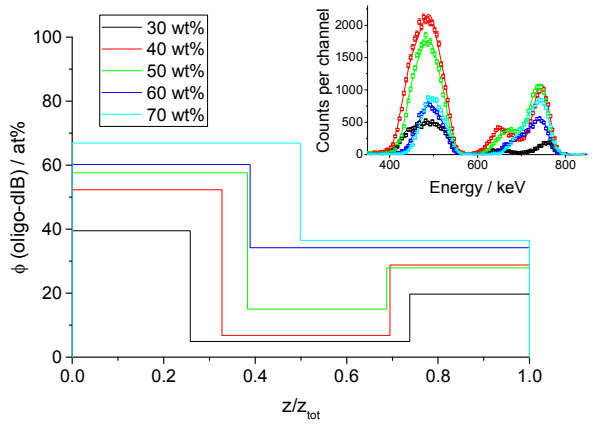

Fig. 8 Elastic recoil detection analysis for 30-70 wt% oligo-dIB in thin PB films. The composition versus depth profiles correspond to the fitted data presented in the inset. The depth scale has been normalized for clarity. Profiles with absolute depth scale are included as supporting information S.I.3.

Discussion

The results presented illustrate some of the remarkably rich range of surface behaviour that exists for binary oligomer / polymer thin film mixtures. Fundamental differences in both the vertical and lateral composition profiles arise from subtle variations in chemical structure or oligomer molecular weight. Therefore, the problem of predicting surface composition and subsequent performance of even the most simplified models for hot melt adhesives is far from trivial. While a modest surface excess of oligomers is highly desirable for improving surface tack in HMAs, a macroscopically thick oligomer-rich layer would drastically undermine the mechanical strength of bonding unless it could be reabsorbed into the bulk. Moreover if the oligomers on the surface can migrate onto other components of a product there may be further unintended consequences, such as contamination of neighbouring surfaces and the loss of flexibility in the adhesive.

We consider the main factors driving surface segregation to be (i) disparity in molecular weight, (ii) difference in surface energy and (iii) incompatibility between components. Other factors such as elasticity,[48] crystallization[12] or deformation may be relevant to more complex matrices, but are not considered here since all of the components are amorphous and have shorter relaxation times than the timescale of observation.

Although our results show several examples of strong surface and interfacial segregation, there are also many examples where this behaviour is virtually absent; therefore while the discrepancy in molecular weight may be a factor in oligomer surface segregation, it cannot be the dominant factor in all cases. In every case we anticipate that the samples are close to equilibrium, since under ambient conditions, all of the components are well above their T_gs. Previous examples of oligomer segregation in polymer films in the literature are sparse, apart from the classic work of Hariharan et al, [49] which showed that (i) disparity in molecular weight could overcome the tendency for deuterated species to segregate to the surface of isotopic blends and (ii) the enrichment of the lower molecular weight component at the surface was only weakly dependent upon the molecular weight of the larger polymer. The length scale of the surface layer defined as τ in equation 2 is dominated by the minority component; or if the volume fractions are similar ($\phi \sim 0.5$) the smaller component. However, for the most extreme disparity of molecular weight in their study (matrix degree of polymerization, DP = 5094, oligomer DP = 115) the difference between surface and bulk volume fraction was 0.3, and the surface excess had a correlation length of 1.8 nm. This surface excess ($z^* \sim 0.6$ nm) is an order of magnitude smaller than we observed for dsq in PB (Figure 3) and in fact would have been difficult to detect except by neutron reflectometry. The absence of any discernible surface excess of dsq in PI when measured by ERDA is perhaps surprising given the much greater discrepancy in molecular weight for our system (~ 370) than for the isotopic blends previously reported (< 50). We therefore explored this system further by neutron reflectometry, which indicated a very slightly enriched surface layer (supporting information S.I.4.) from which we estimate the surface excess to be ~0.16 nm. The thickness of the adsorbed layer is of the order of 0.6 nm, which while close to the resolution of the NR measurement, is consistent with equation 2 for weakly segregating mixtures.

Influence of surface energy

It is well known that a mixture will normally minimize its free energy by segregation of the lower surface energy component to the exposed surface, and similarly polar, high energy components tend to segregate to polar interfaces such as

View Article Online
DOI: 10.1039/C7SM00048K

silica.[50, 51] Unfortunately, it is very difficult to obtain accurate surface energy data for these materials as they fall between the extremes of liquid or solid material, or worse, contain a mixture of both states. For liquids and low molecular weight polymers, surface energy (or surface tension) is directly measureable by methods such as drop shape analysis or for somewhat more viscous materials a micro-Wilhelmy plate.[52] A requirement of these methods is that the material will flow to an equilibrium shape on an experimentally realizable time. In an earlier study on functionalized polybutadienes of almost an order of magnitude lower molecular weight than the PB matrix in this work, it was found that equilibration times for droplets to flow could take days or weeks.[29] Given the well-known $M^{3.4}$ dependence of entangled polymer viscosity on molecular weight, this approach is not feasible for these polymer matrices, and could certainly not be applied to matrices containing copolymers with glassy blocks. The alternative of obtaining solid surface energy via contact angle measurements[12, 53] is also problematic, due to the fact that some displacement of oligomer, local reorganization (e.g. of the pendant vinyl groups in PB), or contamination by the oligomer of the contacting fluid is unavoidable on the timescale of measurement. We therefore briefly consider group contribution to provide a qualitative guide to the order of increasing surface tension. For hydrocarbon polymers, surface energy contributions increase from CH_3 (30 mJ m^{-2}) to CH_2 (36 mJ m^{-2}), with higher values up to 45 mJ m^{-2} for unsaturated species such as aromatic rings.[24] On this basis, we expect the surface energy of the polymer matrix to increase from hPI to PI to PB. Similarly the corresponding values for the oligomers would be expected to increase from oligo-dIB to dsq to oligo-dS, but may be significantly shifted due the influence of density, which is sensitive to molecular weight in this range. Our observation that dsq is much more surface active in PB than in PI suggests that the PB matrix has a greater surface energy than PI. This result is consistent with some literature values[24] for the surface energy of PI and PB (31-34 and 43.1 - 48.6 mJ m^{-2} respectively). However, surface energy data should be treated with some caution since these values are sensitive to microstructure and end-group, and other sources[54] quote very much lower surface energies (25 mJ m^{-2}) for PB with 1,2 addition. Consequently, the effective surface energy of the pure PB will significantly depend on the quantity and distribution of 1,2 units in the chain microstructure. Furthermore, surface energy difference alone should not lead to a complete wetting layer of oligomer; therefore it is important that we consider also the compatibility of the components.

Influence of compatibility

While differences in surface energy of the pure components are expected to direct surface or interfacial segregation of oligomers, it is anticipated that compatibility will also have a strong influence on the extent of surface segregation. In addition to differences in structure previously noted as contributing to surface energy, increasing the molecular weight of the oligomer decreases the entropy of mixing as is apparent from the Ni terms in equation 1. (For the polymers considered here, N2 is always at least 10^3, so the polymer molecular weight in this range is insignificant.) Here, we have carried out the analysis of miscibility with the same deuterium labelled components as were used for surface segregation analysis. This eliminates any artefacts that might arise as a result of deuterium labelling, which slightly reduces the cohesive energy density and surface energy of materials when compared to their hydrogenous counterparts.[10, 49] Table 2 summarizes the overall results obtained by comparing the Fox equation's predictions with the T_g values measured by DSC.

Table 2 Compatibility matrix obtained by comparing DSC data with results expected from the Fox equation.

Compatibility matrix		oligo-dS	oligo-dIB	dsq
	T_g / °C	-13.3	-67.2	-96.8
hPI	-50.8			(ΔT_g > Fox)
PI	-54.6	2 T_g at >70wt%		(ΔT_g > Fox)
PB	-87.9		2 T_g at >50wt%	

Polymer T_g independent of oligomer, denotes incompatible (red), whereas if the T_g more rapidly approaches that of the pure oligomer than predicted by the Fox equation, the system is compatible (green). In intermediate cases where the T_g changes with blend composition, but by less than is predicted by the Fox equation, the system is considered to be partially compatible (amber).

The analysis by DSC provides a direct guide to compatibility, utilising sufficiently small quantities of material to be practical with the small quantities of deuterated components available. We note that for two cases (oligo-dS / PI and oligo-dIB / PB) there appears to be a transition from a single phase mixture to a two phase mixture at high oligomer concentrations. Clearly this indicates that some mixtures are highly incompatible and the tendency to phase separation at high oligomer concentration is qualitatively consistent with the Flory Huggins theory, which predicts the critical composition, ϕ_c, has a high proportion of the oligomer according to[55]

$$\varphi_c = \left[1 + \left(\frac{N_1 v_1}{N_2 v_2}\right)^{\frac{1}{2}}\right]^{-1} \qquad (6)$$

Moreover, by comparing the compatibility of dsq and oligo-dIB, which structures are both saturated alkane chains but different molecular weights, it appears that the higher molecular weight oligomer is always less compatible with the matrix, which is an expected consequence of the $1/N_i$ terms in equation 1.

There is a strong correlation between the mixtures judged to be least compatible by DSC analysis and strong surface segregation behaviour observed for films of these materials. Surface segregation was most apparent for the two least

View Article Online
DOI: 10.1039/C7SM00048K

compatible oligomer/polymer combinations, highlighted in red. Of the compatible (green) mixtures, only dsq/PB showed significant surface segregation. We note also that for mixtures of dsq with either hPI or PI, the T_g shift exceeded the Fox equation prediction for athermal mixing and in these cases, no surface excess was determined. The nature of deviation from the Fox equation is interesting because it appears to correlate well with incompatibility and segregation. The large shift (ΔT_g > Fox) for dsq / PI could suggest a more compatible system than dsq / PB (ΔT_g ~ Fox) since this behaviour is farthest removed from an incompatible system, for which there is no shift in T_g. However, this explanation for the observed trend in surface behaviour is not adequate since it is not consistent with the established relationships between T_g, free volume and compatibility. Briefly, favourable interactions between mixed components should have a negative free volume of mixing, ΔV_{mix}, and this in turn would be associated with an increase in the absolute value of T_g, relative to the prediction of the Fox equation. This effect has been well established for polymer blends by the thermodynamic analysis of Lu and Weiss, which demonstrated that the T_g of blends should increase with increasingly favourable interactions (negative χ).[56, 57] We therefore conclude that while the correlation between compatibility inferred from ΔT_g and surface segregation is useful, a more robust method is needed to predict the wetting behaviour. Furthermore, we note that the DSC analysis is restricted to the region of the glass transition temperatures, which is much lower than the measurement temperature of surface segregation. Given the relatively rapid equilibration that we expect for these small molecule systems, it is likely that there is a significant difference between the temperature of surface segregation analysis and the effective temperature at which compatibility is inferred from DSC.

Hansen solubility parameters can provide some insight into the observed miscibility behaviour of the nonpolar materials under consideration in this work. The Hansen solubility is dominated by the dispersive component, δ_D, which is related to refractive index, n_i, by[58]

$$\delta_D / (\mathrm{MPa})^{\frac{1}{2}} = 9.55\, n_i - 5.55 \qquad (7)$$

The similarity in refractive index values for PB and PI (table 1) suggests that they have almost identical solubility parameters which would imply that the difference in dsq surface segregation between PI and PB matrices arises from differences of surface energy rather than compatibility. However, the accuracy of this interpretation is limited by the accuracy of surface tension or refractive index data for these materials. Recent experimental and computational advances in determining miscibility behaviour both recognize the significance of the volume change of mixing, ΔV_{mix}, on overall miscibility behaviour. Lipson *et al*[20, 59] have successfully used thermodynamic PVT data for pure components and one value for ΔV_{mix} to predict phase behaviour over a large range of parameter space. Interestingly, mixtures can be divided into UCST or LCST systems, depending on whether the favourable energy of interaction between unlike components is less than or greater than the geometric mean of the self-interaction terms respectively.

In the absence of the necessary experimental thermodynamic data (e.g., critical solution temperature, cloud point curve, ΔV_{mix}) for parametrizing these systems, we have used large sets of PVT data to characterize the pure compounds (like interactions) and relied on combining rules to predict the unlike interactions. As it was shown by Lipson et al. [13, 32] that sensitive phase boundaries depend on the unlike interaction, we do not expect quantitative predictions, but analyze relative behaviour inherent in the pure component properties.

For exploring the relative miscibility of squalane/PB and squalane/PI, all three components were parametrized within the SAFT-γ Mie framework based on a large set of density data. Two different experimental data sets were used each for PB and PI, which had close but slightly different monomer ratios compared to the polymers characterized in this work.[44, 46] Only one data set was found for squalane.[45]

The SAFT-γ Mie predictions for the systems in this work show a smaller free energy of mixing for PI/sq compared to PB/sq (incompatibility for PB/sq and partial compatibility for PI/sq), implying that squalane is more compatible with PI than PB, which is verified by the experimental results presented in this work. The difference in solubility is not due to the molecular weight difference between PI and PB, as the SAFT predictions remain almost unchanged when PB is modelled with the same M_w as PI. SAFT-γ Mie predictions using predicted unlike interactions (combining rules) for the relative volume change upon mixing show a volume expansion for both systems.

Additionally the ΔV_{mix} dependency of squalane in PB and PI was explored by MD simulations and SAFT-γ Mie calculations. In MD shorter chain lengths of 12 monomer units for PI and PB were modelled to make the MD simulations computationally accessible. Results show a volume expansion upon mixing, $\Delta V_{mix}/V_{pure}$ (sq / PB) = $4.2\times10^{-4} \pm 1.5\times10^{-4}$, $\Delta V_{mix}/V_{pure}$ (sq / PI) = $6.3\times10^{-4} \pm 1.4\times10^{-4}$. An expansion of volume is also predicted by SAFT for both the reduced polymer weight used in the MD simulation and the experimental M_w. The SAFT model reveals that for both PI/sq and PB/sq the expansion of volume reduces with increasing molecular weight and increasing temperature. There are indications that experimental negative volumes of mixing can be expected for the PB/sq and PI/sq systems: 1. SAFT predicts negative volume of mixing for the experimental M_w systems above 300 – 420 K depending on the parameter set. 2. Fitting the unlike interactions to experimental data would increase compatibility and the unlike interaction and therefore reduce the volume of mixing. The ability to predict the temperature dependence of compatibility is particularly significant to the application of HMAs, due to their need for different surface properties when applied hot to those after bonding at ambient conditions.

As the relative volume of mixing values change with the chosen reference PVT set (and therefore with the SAFT parameter set), no comment can be made on the MD V_{mix} value of PI/sq being larger than of PB/sq. For more confident

View Article Online
DOI: 10.1039/C7SM00048K

predictions of the volumes of mixing of the PB/sq and PI/sq blends in this work, the unlike interactions within SAFT should be fitted to experimental thermodynamic data of the blend, and the polymer molecular weight within MD simulations should be close to the experimental weights.

Quantifying surface segregation.

Turning our attention now to the derived surface concentration profiles we see some quite unexpected results. The fit to the experimental data yields the composition profile shown in the inset of the figure 3, from which z^* (dsq / PB) is calculated to be 24.3 nm. Although the precise thickness of this excess layer is difficult to determine with ERDA due to the limited resolution, the product of concentration and depth is well characterized; therefore surface excess values are normally accurate within the statistics of the measurement, which will be of the order ±10%. The significance of this value for z^* is that it is an order of magnitude greater than the length of the oligomer molecule; therefore can only be accounted for by a thick wetting layer. The formation of a stable surface excess, with a decay length which can persist to depths of tens of nanometers, is normally associated with a clearly phase separated system,[17, 60] or one in which the film is sufficiently thin that the influence of the surfaces on the overall free energy of the system may perturb the phase boundary somewhat.[61] For dsq and PB, the uncertainty in ΔT_g / $\Delta T_{g,max}$ is quite large because $\Delta T_{g,max}$ is relatively small, so it is possible that DSC is unable to resolve coexisting phases with similar T_g values. Further tests on thick samples of hydrogenous squalane and PB appear to show some haziness at high squalane fractions (70%), which disappears when the sample is heated above room temperature (>35 °C). This indicates that squalane / PB is a partially compatible UCST mixture and is consistent with the observed wetting behaviour.

Concentration profiles for incompatible systems

Amongst the less compatible systems identified by DSC, we compare the behaviour of oligo-dIB in thin PI and PB matrices. This oligomer was judged to be marginally more compatible with PI than PB on the basis that there was some shift in T_g of PI with respect to pure PI, whereas the T_g of PB remained unperturbed by the oligomer. The relative compatibility of this unsaturated oligomer with PI and PB is consistent with the order seen for dsq, except that oligo-dIB, having a significantly greater molecular weight is generally less compatible with either polymer matrix. For both mixtures, the large surface and interfacial excesses revealed by ERDA in Figures 6 and 8 exceed what can be accounted for by a single layer; therefore suggest wetting behaviour that is consistent with the two phase mixtures. We have also explored the surface segregation of a higher molecular weight oligo-dIB (2200 g/mol) in PB and found that this is even more segregating than oligo-dIB (900 g/mol), which is consistent with increasing incompatibility with increasing molecular weight. NR data, fits and composition profiles are provided as supporting information, S.I.5.

An interesting distinction between oligo-dIB in PI and the same oligomer in PB is that only in the latter case is an excess of oligomer detected at the buried interface (Figure 8). Here the composition profiles have been presented on a normalized depth scale for clarity. The absence of any detected interfacial excess at the very highest oligomer concentrations is most likely due to these films being somewhat thinner than the more polymer-rich films. The presence of oligo-dIB at the surface of either film is consistent with the expectation that this saturated low molecular weight oligomer has a significantly lower surface energy than either polymer matrix. However, given the propensity of polar, high surface energy components to segregate to buried interfaces of films,[51] the accumulations of oligo-dIB at this interface is not expected on the basis of surface energy arguments. Given the similarity of solubility parameter for these polymers, it is not obvious why they should have significantly different interactions with the substrate. The composition profiles seen are in fact more consistent with the oscillating profiles seen for surface-directed spinodal decomposition, and may in this case simply arise in PB but not PI because of the timescale of equilibration during solvent evaporation.[62, 63] Although beyond the scope of this present work, we note that the timescale of development of such spinodal waves could provide valuable insights into the stability and rate of toughening of adhesive formulations.

Surface topography

Although it is impossible to determine absolute surface concentrations because of the limited depth resolution of ERDA, the relatively diffuse profiles suggested for oligo-dIB in PI (Figure 6), suggest that the surface layer is not pure oligomer. Because Flory Huggins (equations 1 and 6) predicts a coexistence in which the oligomer rich phase is almost devoid of polymer, our results suggest that the composition profile inferred from ERDA is not laterally homogeneous. AFM was performed on thin (~100 nm) of 30 wt% oligo-dIB in PI (Figure 7) confirms that these samples do indeed contain significant lateral structure, with disk-like islands of adhesive (oligo-dIB-rich) material dispersed in a more elastic (PI-rich) material. The disks are ~7 μm in diameter and are raised ~10 nm with respect to the adjacent film (Figure 9) – i.e. a tenth of the total thickness of the film. The diameter of the disks far exceeds the total film thickness; which is a feature of lateral phase separation in polymer films of surface active mixtures. There is no total coverage of the PI-rich phase by the oligo-dIB rich phase. Some of the disks are overlapping which suggests that they might have grown from an initial spot and extended by lateral migration on the surface. Although the origin and growth mechanism of the laterally separated domains is not discernible from these data, we note that similar structures are possible, even for polymers of quite similar surface energy when formed by spin-coating.[33, 64, 65] ERDA data, recording an average composition at the surface, should have recorded a surface excess in the first tenth of the total sample thickness.

View Article Online
DOI: 10.1039/C7SM00048K

However, the length scale is much larger on the concentration profiles recorded (Figure 5). This implies that the oligomer-rich structure extends well below the surface of the "disks", as annotated on figure 9.

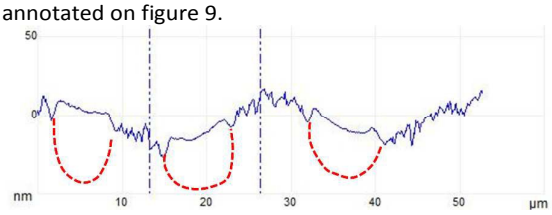

Fig . 9 Cross section of AFM height profile of a ~100 nm film of 30% oligo-dIB in PI. The dotted curves indicate the extent of the oligo-dIB inferred from ERDA.

Remarkably, given that both film components are at least 75 °C above their respective T_g values at the measurement temperature, the structures appear to be quite stable, and no coarsening was observed over several hours. The time needed to install the sample on the AFM device and obtain a first scan is around 10 minutes. It appears that the equilibrium state (or at least a metastable state) is reached within less than 10 minutes; soon after the solvent has evaporated. Unfortunately it was not possible to apply this analysis to the dsq / PB system because of the highly fluid nature of dsq, but the successful specular NR experiments suggest that there is little lateral variation in these samples.

Conclusions

We report the impact of the molecular weight, surface energy and compatibility between non-polar oligomeric additives and amorphous polymer matrices on the vertical depth distribution of the oligomer in thin polymer films. Through DSC measurements and evaluation of the T_g of blends of several compositions, the compatibility of the oligomer/polymer pair was systematically assessed for a matrix of 3 polymers and 3 oligomers and found to correlate strongly with surface or interfacial segregation. The surface segregation behaviour of four systems, presenting different compatibility behaviours were studied in detail by ERDA and NR to measure the vertical partitioning of the oligomer in the thin polymer films. The most compatible systems (dsq in PI) presented an even distribution over the whole film thickness with very little surface or interfacial enrichment of either component. A significant surface excess was observed for dsq in PB, which DSC and turbidimetry indicates is a less compatible system than dsq in PI. Computational calculations using SAFT-γ and MD support the DSC compatibility analysis and enable extrapolation to the temperature range relevant for the HMA applications. This approach can also be used where DSC is unsuitable; for example where the T_g of both components is very similar. For systems in the two phase regime, a phase separation occurs at the surface and a "wetting layer" can be formed, and in the case of oligo-dIB / PI, clear lateral segregation into 'islands' was also evident by AFM. Despite both components in this film being well above their T_g, no coarsening or evolution of this structure was observed over many hours, indicating that even these simple model systems can exhibit complex non-equilibrium behaviour. Surface segregation of the oligomer is mainly directed by the surface energy difference between the oligomer and the matrix with saturated oligomers, dsq and oligo-dIB tending to segregate to exposed surfaces and unsaturated oligo-dS segregating to the buried interface of hPI films. However, the extent of segregation is overwhelmingly due to the incompatibility between the oligomer and the polymer. In the case of strongly incompatible oligo-dIB in PB films, segregation to both surface and buried interfaces was apparent, possibly due to a spinodal wave formed during initial stages of solvent evaporation separation, which was kinetically trapped in the dry film. The tendency of small molecules to segregate to surfaces or interfaces of mixtures with larger polymers, although well established for nearly ideal isotopic blends is insignificant when compared to other factors, notably the compatibility of the mixed components.

Acknowledgement

We are grateful to the European Commission (through the Marie Sklodowska-Curie actions) for funding this project and to Procter and Gamble (Germany) our partner and Dr Todd Mansfield (P&G Cincinnati) for provision of the PI and hPI materials and for helpful discussions. We are also grateful to We thank STFC for provision of the ISIS neutron reflectometry facilities and beamtime awards RB1520358 and RB1510402, was provided by STFC. We thank Arron Briddick, Rebecca Fong and Salvatore Croce for helping with the NR experiments and Dr Buddhapriya Chakrabarti (Durham University) and Dr. Gabriela Schäfer (P&G Germany) for many helpful and stimulating discussions.

References

1. W. Li, L. Bouzidi and S. S. Narine, *Ind Eng Chem Res*, 2008, **47**, 7524-7532.
2. I. Benedek and M. M. Feldstein, *Handbook of Pressure-Sensitive Adhesives and Products: - Three Volume Set*, Taylor & Francis, 2008.
3. C. Creton, E. Papon and M. R. Society, *Materials Science of Adhesives: How to Bond Things Together*, 2003.
4. D. A. Dillard, *The mechanics of adhesion*, Elsevier, 2002.
5. P.-G. d. Gennes, in *Simple Views on Condensed Matter*, pp. 405-409.
6. M. T. Degiacomi, V. Erastova and M. R. Wilson, *Computer Physics Communications*, 2016, **202**, 304-309.
7. G. O. Yahya, S. K. A. Ali and E. Z. Hamad, *Polymer*, 1996, **37**, 1183-1188.
8. H. L. Frisch and S. Al-Madfai, *J. Am. Chem. Soc.*, 1958, **80**, 3561-3565.
9. A. Hariharan, S. K. Kumar and T. P. Russell, *Macromolecules*, 1991, **24**, 4909-4917.
10. R. A. L. Jones, E. J. Kramer, M. H. Rafailovich, J. Sokolov and S. A. Schwarz, *Phys. Rev. Lett.*, 1989, **62**, 280-283.

View Article Online
DOI: 10.1039/C7SM00048K

11. P. A. V. O'Rourke-Muisener, J. T. Koberstein and S. Kumar, *Macromolecules*, 2003, **36**, 771-781.
12. S. J. Hardman, L. R. Hutchings, N. Clarke, S. M. Kimani, L. L. E. Mears, E. F. Smith, J. R. P. Webster and R. L. Thompson, *Langmuir*, 2012, **28**, 5125-5137.
13. J. F. Elman, B. D. Johs, T. E. Long and J. T. Koberstein, *Macromolecules*, 1994, **27**, 5341-5349.
14. M. Wolff, P. Kuhns, G. Liesche, J. F. Ankner, J. F. Browning and P. Gutfreund, *Journal of Applied Crystallography*, 2013, **46**, 1729-1733.
15. V. S. Minnikanti and L. A. Archer, *Macromolecules*, 2006, **39**, 7718-7728.
16. S. Dietrich, *Phase transitions and critical phenomena*, Academic Press, 1988.
17. H. Wang, J. F. Douglas, S. K. Satija, R. J. Composto and C. C. Han, *Phys Rev E*, 2003, **67**, 6.
18. M. L. Huggins, *The Journal of Chemical Physics*, 1941, **9**, 440-440.
19. P. J. Flory, *The Journal of Chemical Physics*, 1942, **10**, 51-61.
20. J. S. Higgins, J. E. G. Lipson and R. P. White, *Philosophical Transactions of the Royal Society a-Mathematical Physical and Engineering Sciences*, 2010, **368**, 1009-1025.
21. A. Hariharan, S. K. Kumar and T. P. Russell, *Macromolecules*, 1990, **23**, 3584-3592.
22. M. Geoghegan, T. Nicolai, J. Penfold and R. A. L. Jones, *Macromolecules*, 1997, **30**, 4220-4227.
23. D. J. Worsfold and S. Bywater, *Can. J. Chem.-Rev. Can. Chim.*, 1964, **42**, 2884-&.
24. J. Brandrup and E. H. Immergut, eds., *Polymer Handbook*, 3rd edn., Wiley, New York, 1989.
25. V. Galiatsatos, R. O. Neaffer, S. Sen and B. J. Sherman, ed. J. E. Mark, American Institute of Physics, Woodbury, New York, 1996, pp. 535-543.
26. N. Tripathi, *International Journal of Thermophysics*, 2005, **26**, 693-703.
27. R. J. Composto, R. M. Walters and J. Genzer, *Materials Science and Engineering R*, 2002, **R38**, 107-180.
28. R. L. Thompson, in *Polymer Science: A Comprehensive Reference*, eds. M. Moeller and K. Matyjaszewski, Elsevier BV, Amsterdam, 2012, vol. 2, pp. 661-681.
29. S. M. Kimani, S. J. Hardman, L. R. Hutchings, N. Clarke and R. L. Thompson, *Soft Matter*, 2012, **8**, 3487-3496.
30. C. Jeynes, N. P. Barradas and E. Szilágyi, *Anal. Chem.*, 2012, **84**, 6061-6069.
31. C. Jeynes, M. J. Bailey, N. J. Bright, M. E. Christopher, G. W. Grime, B. N. Jones, V. V. Palitsin and R. P. Webb, *Nucl. Instrum. Methods Phys. Res. Sect. B-Beam Interact. Mater. Atoms*, 2012, **271**, 107-118.
32. N. P. Barradas and C. Jeynes, *Nucl. Instrum. Methods Phys. Res. Sect. B-Beam Interact. Mater. Atoms*, 2008, **266**, 1875-1879.
33. C. D. James, C. Jeynes, N. P. Barradas, L. Clifton, R. M. Dalgliesh, R. F. Smith, S. W. Sankey, L. R. Hutchings and R. L. Thompson, *Reactive and Functional Polymers*, 2015, **89**, 40-48.
34. C. Jeynes, N. P. Barradas, P. K. Marriott, G. Boudreault, M. Jenkin, E. Wendler and R. P. Webb, *J. Phys. D-Appl. Phys.*, 2003, **36**, R97-R126.
35. D. G. Bucknall, S. A. Butler and J. S. Higgins, in *Scattering from Polymers*, 2000, vol. 739, pp. 57-73.
36. C. D. James, C. Jeynes, N. P. Barradas, L. Clifton, R. M. Dalgliesh, R. F. Smith, S. W. Sankey, L. R. Hutchings and R. L. Thompson, *React. Funct. Polym.*, 2015, **89**, 40-48.
37. A. Briddick, P. Li, A. Hughes, F. Courchay, A. Martinez and R. L. Thompson, *Langmuir*, 2016, **32**, 864-872.
38. A. Nelson, *J Appl Crystallogr*, 2006, **39**, 273-276.
39. B. Hess, C. Kutzner, D. van der Spoel and E. Lindahl, *Journal of Chemical Theory and Computation*, 2008, **4**, 435-447.
40. C. Jeynes and J. L. Colaux, *Analyst*, 2016.
41. V. Papaioannou, T. Lafitte, C. Avendaño, C. S. Adjiman, G. Jackson, E. A. Müller and A. Galindo, *The Journal of Chemical Physics*, 2014, **140**, 054107.
42. T. Lafitte, A. Apostolakou, C. Avendaño, A. Galindo, C. S. Adjiman, E. A. Müller and G. Jackson, *The Journal of Chemical Physics*, 2013, **139**, 154504.
43. S. Kawahara, S. Akiyama and A. Ueda, *Polym J*, 1989, **21**, 221-229.
44. D. J. Walsh and P. Zoller, *Standard Pressure-Volume-Temperature Data for Polymers*, CRC Press, Technomic Publishing, Lancaster, PA, 1995.
45. O. Fandiño, A. S. Pensado, L. Lugo, M. J. P. Comuñas and J. Fernández, *Journal of Chemical & Engineering Data*, 2005, **50**, 939-946.
46. Y. X. Yi and P. Zoller, *Journal of Polymer Science Part B: Polymer Physics*, 1993, **31**, 779-788.
47. A. N. Gaikwad, E. R. Wood, T. Ngai and T. P. Lodge, *Macromolecules*, 2008, **41**, 2502-2508.
48. J. Krawczyk, S. Croce, T. C. B. McLeish and B. Chakrabarti, *Phys. Rev. Lett.*, 2016, **116**.
49. A. Hariharan, S. K. Kumar and T. P. Russell, *J. Chem. Phys.*, 1993, **98**, 4163-4173.
50. P. A. V. O'Rourke-Muisener, C. A. Jalbert, C. G. Yuan, J. Baetzold, R. Mason, D. Wong, Y. J. Kim and J. T. Koberstein, *Macromolecules*, 2003, **36**, 2956-2966.
51. L. R. Hutchings, C. J. R. Douglas, C. L. Rhodes, W. D. Carswell, M. W. A. Skoda, J. R. P. Webster and R. L. Thompson, *Langmuir*, 2010, **26**, 15486-15493.
52. Z. Qian, V. S. Minnikanti, B. B. Sauer, G. T. Dee, W. G. Kampert and L. A. Archer, *Journal of Polymer Science Part B: Polymer Physics*, 2009, **47**, 1666-1685.
53. M. Żenkiewicz, *Journal of Achievements in Materials and Manufacturing Engineering*, 2007, **24**, 137-145.
54. M. J. Owen, ed. J. E. Mark, American Institute of Physics, Woodbury, New York, 1996, pp. 669-676.
55. N. P. Balsara, in *Physical Properties of Polymers Handbook*, ed. J. E. Mark, American Institute of Physics, Woodbury, New York, 1996, pp. 257-268.
56. X. Lu and R. A. Weiss, *Macromolecules*, 1992, **25**, 3242-3246.
57. X. Lu and R. Weiss, *Macromolecules*, 1993, **26**, 248-248.
58. Y. Du, Y. Xue and H. L. Frisch, ed. J. E. Mark, American Institute of Physics, Woodbury, New York, 1996, pp. 227-239.
59. R. P. White, J. E. G. Lipson and J. S. Higgins, *Macromolecules*, 2012, **45**, 1076-1084.
60. L. J. Norton, E. J. Kramer, F. S. Bates, M. D. Gehlsen, R. A. L. Jones, A. Karim, G. P. Felcher and R. Kleb, *Macromolecules*, 1995, **28**, 8621-8628.
61. D. Kawaguchi, M. Ohya, N. Torikai, A. Takano and Y. Matsushita, *Polym. J*, 2007, **39**, 1274-1280.

View Article Online
DOI: 10.1039/C7SM00048K

62. G. Krausch, C. A. Dai, E. J. Kramer, J. F. Marko and F. S. Bates, *Macromolecules*, 1993, **26**, 5566-5571.
63. R. A. L. Jones, L. J. Norton, E. J. Kramer, F. S. Bates and P. Wiltzius, *Phys. Rev. Lett.*, 1991, **66**, 1326-1329.
64. P. Mokarian-Tabari, M. Geoghegan, J. R. Howse, S. Y. Heriot, R. L. Thompson and R. A. L. Jones, *Eur. Phys. J. E*, 2010, **33**, 283-289.
65. S. Y. Heriot and R. A. L. Jones, *Nat Mater*, 2005, **4**, 782-786.

View Article Online
DOI: 10.1039/C7SM00048K

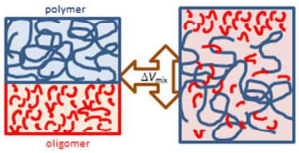

Oligomer segregation is acutely sensitive to tiny changes in compatibility or volume of mixing